

RHIC Beam Experiments for the LHC Era

W. Fischer* and F. Zimmermann†

October 15, 1999

Abstract

RHIC will offer the possibility to investigate in more detail a number of particle beam phenomena that are of interest in the LHC era. This is partly due to RHIC's parameter range and partly due to new and innovative diagnostics equipment that will be installed in the rings. In this report, we motivate and outline several machine experiments. These experiments concern weak-strong and strong-strong beam-beam interaction, electron clouds, the dynamic aperture, intrabeam scattering, and the ring circumference.

1 Introduction

Accelerators of the LHC era are faced with a number of new challenges as their parameters are pushed to provide for higher energies and luminosities. RHIC is a test bench for the investigation of phenomena that limit these efforts since it is one of only two hadron colliders in existence and the only one that can collide two hadron beams of relatively high intensity. Tab. 1 shows relevant RHIC machine parameters for gold operation [1].

Table 1: RHIC parameters for gold operation [1].

| Parameter | Symbol | Value |
|--------------------------------------|--------------------|--|
| Circumference | C | 3.8 km |
| Betatron tunes | $Q_{x,y}$ | 29.18, 28.19 |
| Ion species | – | gold |
| Atomic number | Z | 79 |
| Mass number | A | 197 |
| Bunch population | N_b | 10^9 |
| Normalized emittance ($1\ \sigma$) | $\epsilon_N^{x,y}$ | $1.7\text{--}6.7\ \mu\text{m}$ |
| Lorentz factor | γ | 12.6 (injection), 100 (top energy) |
| IP beta function | $\beta_{x,y}^*$ | 10 m (injection), 1 m (top energy) |
| Average beta function in arcs | $\beta_{x,y}$ | 30 m |
| rms bunch length [†] | σ_z | 0.4 m (injection), 0.25 m (top energy) |

[†]The bunch length quoted for top energy corresponds to a beam filling the entire 200-MHz rf bucket.

In addition, a number of new and innovative beam diagnostics devices will allow new types of experiments. These are: turn-by-turn ionization profile monitors [2] (installed and tested), AC dipoles [3, 4] (under construction) and a pulsed quadrupole [5] (proposed).

*BNL, Upton, New York

†CERN, Geneva, Switzerland

2 Weak-Strong Beam-Beam Effects

The LHC will enter a new regime of beam-beam interaction, where the effect of the 16 parasitic long-range encounters on either side of each interaction point is the dominant perturbation, rather than the head-on collision. (Perhaps wrongly, we use the term ‘head-on’ collision also when in reality the beams collide under a small crossing angle. The latter is not included in our 4-dimensional computer model.) In simulations for both SSC [6] and LHC [7, 8], the long-range collisions give rise to a well defined diffusive aperture x_{da} . For the nominal LHC parameters the diffusive aperture is about 6σ , as illustrated in Fig. 1.

The diffusion rate, plotted along the vertical axis, refers to the average increase per turn of the rms action for 100 particles launched with equal betatron oscillation amplitudes and random betatron phases. The rms spread is computed as a running average over 1000 turns, in order to suppress regular fluctuations. The initial oscillation amplitudes in the horizontal and vertical plane are chosen to be the same. The diffusion rate is measured in units of $10^8/\epsilon$ (ϵ being the rms emittance). A value ‘1’ on the vertical axis means that the rms action spread of a group of particles grows from zero to a value equal to the rms beam emittance within 10^8 turns, which amounts to 2.5 hours for the LHC, and 20 minutes for RHIC. Diffusion rates larger than ‘1’ should be observed easily.

Fig. 1 shows that, for the LHC, the diffusive aperture is roughly 3σ smaller than the beam-beam separation x_{sep} ($x_{sep} \approx 9.5\sigma$). Beyond this aperture, the diffusion is increased by many orders of magnitude, and, in conjunction with magnetic field nonlinearities, it will result in rapid particle loss.

A simple scaling argument for a $1/r$ force [6] predicts that the distance of the diffusive aperture to the beam-beam separation is proportional to the square root of the bunch current [6, 8], or

$$x_{da} = x_{sep} - \Delta \quad (1)$$

with

$$\frac{\Delta}{\sigma} \propto \sqrt{\frac{N_b}{A\epsilon_N}} Z \quad (2)$$

where σ denotes the rms beam size, N_b the number of particles in the bunch, ϵ_N the normalized emittance, Z the atomic number, and A the mass number. In particular, the aperture reduction Δ is independent of the beta function at the main interaction point (IP), and also independent of the beam energy. It does depend strongly on the normalized emittance and on the atomic number.

Because of the large bunch spacing, at RHIC there are no parasitic beam-beam encounters with 60 bunches [9]. Nevertheless, an equivalent long-range effect can be obtained by separating the two colliding beams at the main interaction points by about 10σ . Fig. 2 shows a few typical simulation results for RHIC, assuming a beam-beam separation of 10σ at two IPs (no collisions in the other IPs). The left picture refers to the nominal bunch population of $N_b = 10^9$ gold ions for the opposing beam. The right picture is for a 100 times larger bunch charge: $N_b = 10^{11}$. As expected, the diffusive aperture is the same at injection and at top energy. Clearly visible, in the right picture, are steep increases of the diffusion at an amplitude of about $6\text{--}7\sigma$. This is quite reminiscent of the LHC simulations in Fig. 1 [8]. If the beam emittance is larger the diffusive aperture is located further outside, in accordance with our above scaling. For the nominal charge, in the left picture, the diffusive aperture is less pronounced. Still, the diffusion rate increases by many orders of magnitude as the oscillation amplitude approaches the opposing beam.

For simplicity, an experiment can be conducted with a small number of bunches, and (long-range) collisions in only one or two IPs. At the other IPs the beams may be completely separated. The current difference between the two beams should be a factor of two or more, in order to suppress strong-strong beam-beam effects, which otherwise might be present as well (see later). The quantity to be measured is the diffusive aperture experienced by the weaker beam. If the beam lifetime is dominated by scattering processes, it is roughly inversely proportional to the aperture and a good indicator. To determine the amplitude-dependent diffusion rate transverse turn-by-turn profiles from the residual-gas

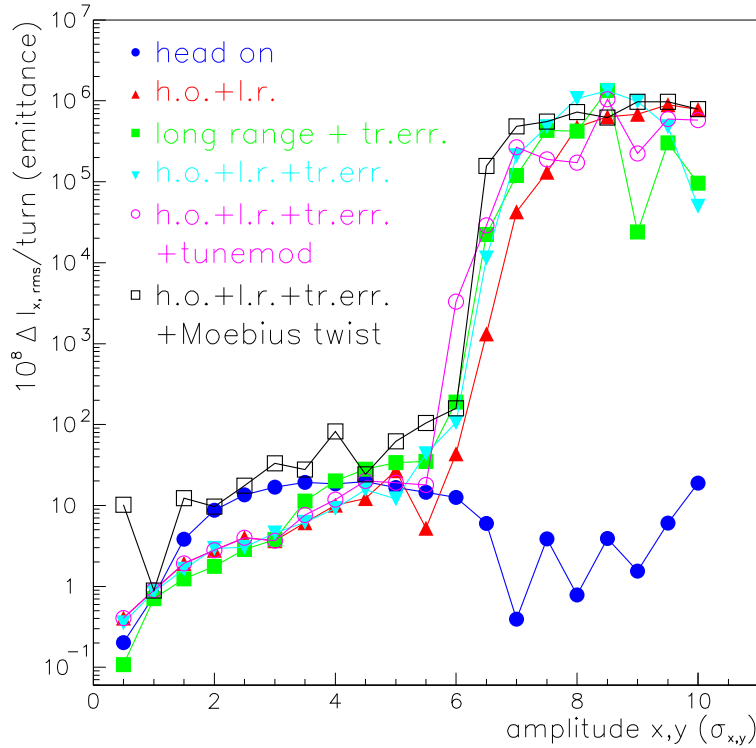


Figure 1: Simulated change of action variance per turn as a function of starting amplitude, for the LHC [8]. Compared are different combinations of head-on collisions, long-range collisions, triplet-field errors, tune modulation, and Moebius twist.

ionization monitor [2] or collimators [10]. Transverse white noise excitation applied to the weak beam will improve the measurement resolution.

3 Strong-Strong Beam-Beam Effects

In the case of two colliding bunches, two coherent oscillation modes exist: a σ mode where the two bunches oscillate in phase, and a π mode, where the two bunches oscillate with respect to each other. The frequency of the σ mode equals the unperturbed betatron tune (in the absence of collisions), whereas the frequency of the π mode is shifted. In case of proton-proton (or gold-gold) collisions, the frequency of the π mode is shifted downwards, because the beam-beam collisions are defocusing.

Using an analytical approach developed by Yokoya and coworkers [11], Alexahin predicted that the coherent π mode in the LHC will not be Landau damped, if the currents in the two beams are the same to within 40%, and if the two tunes are equal. The reason is that under these conditions the coherent tune shift (involving the so-called Yokoya factor) is larger than the incoherent tune spread. No analytical theory exists on the stabilizing or destabilizing effect of long-range collisions.

Recent simulation studies [13] confirm Alexahin's prediction, that the π mode is undamped for the nominal LHC parameters. A typical simulation result for head-on collisions with equal charge is shown

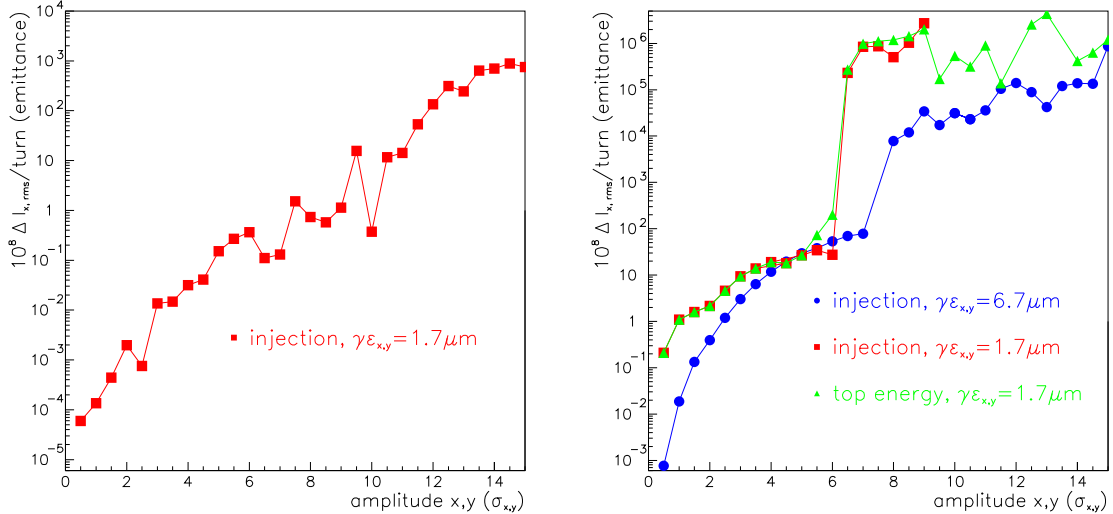


Figure 2: Simulated action diffusion rates in RHIC, with 10σ beam separation at two IPs, as a function of the starting amplitude. The simulation assumes gold ions, with a bunch population of $N_b = 10^9$ [left] and $N_b = 10^{11}$ [right]; betatron tunes $Q_x = 29.18$ and $Q_y = 28.19$; and different normalized emittances as indicated. The planes of separation are alternating: horizontal at one IP and vertical at the other.

in Fig. 3. The simulations also suggest that the long-range collisions will not stabilize the π mode, but on the contrary destabilize it further. As a possible cure, Hofmann proposed to separate the tunes in the two rings [14]. If the tune split of the two rings is larger than the beam-beam tune shift (multiplied by the number of collision points), the oscillations in the two rings are essentially decoupled, and the former π mode is shifted back into the continuum tune spread of either beam, and becomes Landau damped. Simulation results indicate that this cure is efficient [13]. However, since both theory and simulations rely on various approximations and assumptions, an experimental study of the π mode stability is needed.

In a machine experiment, the self-excitation or damping of the π mode can be observed as a function of the current ratio of the two beams, and, for equal currents, as a function of the tune difference between the rings. At the start of collisions, the beam-beam tune shift in RHIC is

$$\xi = \frac{r_p Z^2 N \beta^*}{2\pi\gamma A \sigma_{x,y}^* (\sigma_x^* + \sigma_y^*)} \approx 2 \times 10^{-3} \quad (3)$$

where A denotes the mass number, Z the atomic number, and we have assumed gold ions. Thus, to clearly observe the effect of the decoupling, in the experiment the tune split ΔQ should be varied from 0 to at least 0.005 times the number of collision points. For each working point, the response to a tune excitation reveals the damping or non-damping of the π mode. This experiment can be performed both with head-on collisions, for which we have analytical predictions, and with a transverse beam-beam separation of a few σ . The latter case will allow us to study the coherent beam-beam modes which are supported by the long-range collisions.

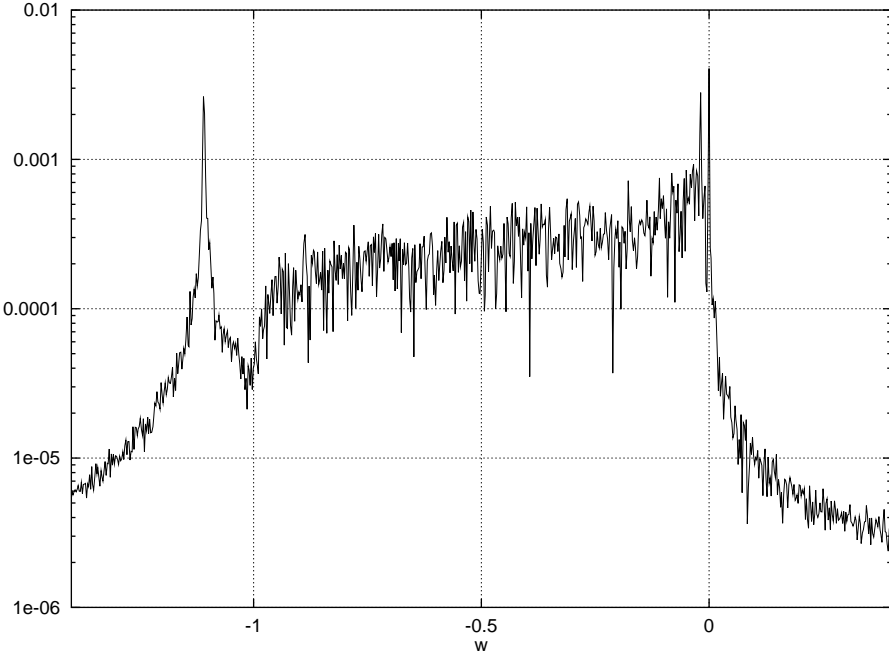


Figure 3: Simulation of coherent beam-beam modes at the LHC [13]: frequency spectrum of the bunch centroid motion (over 2^{17} turns, $N = 10^4$ macro particles). The horizontal axis gives the tune shift from the unperturbed tune Q in units of ξ , i.e. $w = \frac{\nu - Q}{\xi}$. The vertical axis is the corresponding amplitude in logarithmic scale. The π - and σ -oscillation modes are clearly visible.

4 Electron Cloud

The build-up of an electron cloud in the LHC beam pipe can induce a significant heat load on the vacuum chamber wall as well as a transverse multibunch instability [15–18]. Recently, a strong pressure rise has been observed in the CERN SPS when operated with the LHC test beam (84 bunches with 25 ns spacing). The onset of the pressure rise depends strongly on the bunch population and on the length of the LHC bunch train. The phenomenon is attributed to a multipacting electron cloud, that rapidly grows during the bunch train passage. The fast growth indicates a large secondary emission yield of the beam pipe surface. The SPS vacuum chamber is made from stainless steel without any coating.

The multipacting condition reads [15]

$$ZN_b = \frac{b^2}{r_e \Delta s} \quad (4)$$

where Δs is the bunch spacing, Z the atomic number, r_e the classical electron radius, and b the beam pipe radius. Although the simple multipacting picture is oversimplified, perhaps the above equation may give a rough indication of the scaling behavior. With 60 uniformly placed bunches, the bunch spacing in RHIC is about 10 times the LHC spacing. Since the chamber radius is nearly twice that of the LHC, the ‘equivalent’ current ($N_b Z$) would be about a half or a third of the LHC current, i.e. a few times 10^{10} .

However, the situation is more complicated than this. Due to the larger beam pipe radius, electrons at the chamber wall will gain much less energy when a bunch passes by than those at the LHC. For the smaller electron energy, the secondary emission yield is reduced, and, hence, fewer secondary electrons are produced when the primary electrons impinge on the wall. In addition, since the bunch spacing is

Table 2: Simulated heat load induced by electron cloud under various conditions, assuming a maximum secondary emission yield of $\delta_{max} = 2.5$, and a primary ionization-electron yield of $Y_{pe} = 0.03$ per meter.

| Condition | Heat load |
|--|-----------|
| 60 bunches, $ZN_b = 10^{11}$, injection | 2.1 mW/m |
| 60 bunches, $ZN_b = 2 \times 10^{10}$, injection | 0.1 mW/m |
| 60 bunches, $ZN_b = 10^{11}$, top energy | 2.2 mW/m |
| 120 bunches, $ZN_b = 10^{11}$, injection | 9.1 mW/m |
| 240 bunches, $ZN_b = 10^{11}$, injection | 131 mW/m |
| 360 bunches, $ZN_b = 3 \times 10^{10}$, injection | 3.4 mW/m |
| 360 bunches, $ZN_b = 10^{11}$, injection | 1138 mW/m |

larger, a bigger fraction of electrons is lost, before the next bunch arrives. Therefore, we expect that the electron cloud at RHIC is much weaker than in the LHC case. This was also the result of earlier studies [19].

Although unlike for the LHC (but like the SPS) there are no photoelectrons, in RHIC a fairly large number of electrons may be produced by gas ionization. A typical ionization cross section for relativistic singly charged particles is 2 Mbarn. For gold ions, the cross section is enhanced by a factor Z^2 ; it is about $\sigma_{ion} \approx 1.2 \times 10^{-14} \text{ cm}^2$. At a pressure of 1 nTorr and a temperature 4 K, the molecular density of the vacuum is $2.5 \times 10^{15} \text{ m}^{-3}$. The number of ions and ionization electrons generated by one gold atom per meter is then about 0.003. If the actual pressure in the cold sections is not 1 nTorr, but below 10^{-11} nTorr [1], the ionization-electron yield could be 100 times smaller than estimated.

A computer simulation [16, 17] takes into account most of the above effects. As input parameters, we assume an average rms beam size in the arcs of 2 mm at injection (1.4 mm at top energy), and an rms bunch length of 0.4 m (0.25 m at top energy). In addition, we use a maximum secondary emission yield of $\delta_{max} = 2.5$, which is much larger than for the LHC beam pipe. Simulation results are shown in Fig. 4. The longitudinal charge density of the electron cloud is of the order of 10^8 per meter. The situations at injection and at top energy (not shown) are nearly indistinguishable. For the nominal bunch spacing, the electron cloud disappears almost completely before the next bunch arrives, both for a bunch charge $ZN_b = 10^{11}$, illustrated in the top left picture, and for a reduced charge of 2×10^{10} (top right picture). As illustrated by the two center and the bottom left pictures, for shorter bunch spacing there can be a significant accumulation of electrons, and the cloud density increases considerably. Finally, we have simulated the case of 360 bunches with a third of the charge per bunch, $ZN_b = 3 \times 10^{10}$, which is illustrated in the bottom right picture. This last case might be realized by fast de- and rebunching with the 28-MHz rf system.

The simulated heat load is 2.1 mW/m and 2.2 mW/m for the nominal parameters at injection and top energy, respectively. Similar numbers were obtained in Ref. [19]. For 1/5th the current, the heat load decreases to 0.1 mW/m. This is slightly higher than expected if the heat load was due to the primary electrons alone (in which case there would be a cubic dependence of the heat load on the bunch charge). Finally, for a reduced bunch spacing of 32 m (or 120 uniformly placed bunches), the heat load increases to 9.1 mW/m. Much larger values are obtained for even shorter bunch spacings. For 240 and 360 equidistant bunches, the heat loads are comparable to those predicted for the LHC. Simulated heat loads for various cases are listed in Tab. 2.

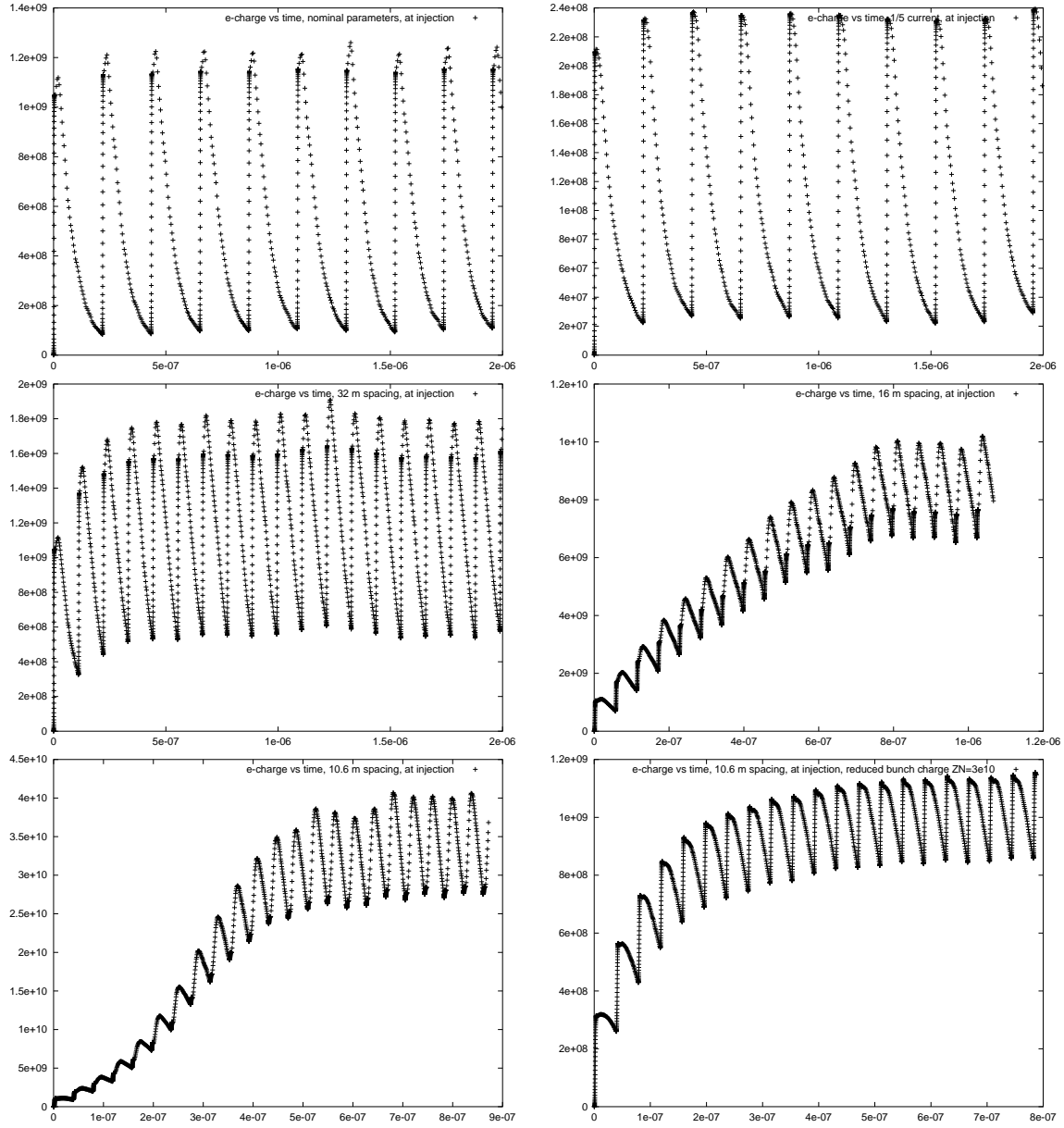


Figure 4: Simulated electron cloud build-up in RHIC. Shown is the total charge of the electron cloud in a 10-m long dipole section as a function of time, during a bunch train passage. A primary ionization electron yield of $Y_{pe} = 0.03$ over a 10-m length is assumed, and a maximum secondary emission yield of $\delta_{max} = 2.5$ at 300 eV. Image charges are not included; however, space-charge forces are. Top left: nominal injection parameters; top right: reduced bunch charge ($Z N_b = 2.5 \times 10^{10}$) and nominal spacing; center left: 1/2 bunch spacing (120 bunches); center right: 1/4 bunch spacing (240 bunches); bottom left: 1/6 bunch spacing (360 bunches); bottom right: 1/6 bunch spacing and reduced bunch charge (360 bunches and $Z N_b = 3 \times 10^{10}$).

5 Dynamic Aperture and Nonlinear Dynamics

Carefully performed element-by-element tracking is now able to reproduce measured dynamic apertures within 30% [20–23]. However, these attempt are only successful if the nonlinear properties of the accelerator are accurately modeled. Techniques to determine experimentally the nonlinear coefficients of a one-turn map are therefore highly desirable. The knowledge of these coefficients may also allow for an effective compensation of resonances that dominate the dynamic aperture.

The AC quadrupole in RHIC is one instrument with which nonlinear coefficients of the accelerator Hamiltonian can be determined in a non-destructive manner [3,4]. Another way is to reconstruct the nonlinear Hamiltonian from turn-by-turn orbit data for a kicked beam. This requires two (non-degenerate) beam-position monitors capable of sampling orbit data over successive turns. Following the early work of Bengtsson [24], and making use of new techniques for precision tune evaluation [25, 26], the SUSSIX program [27] of Bartolini and Schmidt calculates the amplitude and phase of higher-order spectral lines, which are directly related to the Hamiltonian [28]. So far, this program has been applied to orbit data from the SPS and LEP [29], as well as from the KEK/ATF Damping Ring [30]. Detuning with amplitude and resonance driving terms inferred from the measured turn-by-turn orbits may be compared with those obtained from tracking data so that an accelerator model can be validated or rejected. Fig. 5 shows typical a simulation result for the ATF Damping Ring. In all cases studied up to now, the measured tune shift with amplitude agrees well with the model. Some of the resonance driving terms are different from the expectation, however.

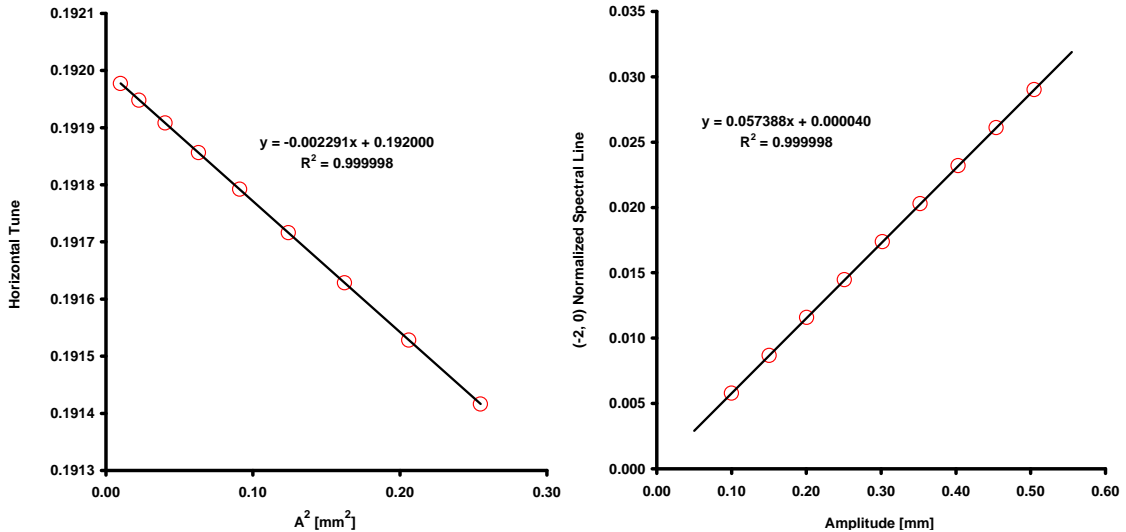


Figure 5: Simulated detuning with amplitude [left] and normalized $(-2,0)$ spectral line [right] as a function of the oscillation amplitude, for the ATF Damping Ring [30].

6 Intrabeam Scattering

Intrabeam scattering is a strong effect in RHIC and it is expected that it will lead to operational limitations at injection and storage. A quantitative test of the existing theories on emittance growth and beam profile as developed in references [31–36] will therefore lead to a better understanding of intra beam scattering effects and hopefully to a better accelerator performance.

Another interesting topic waiting for exploration is the interplay of intrabeam scattering with nonlinear dynamics, *e.g.* due to magnet nonlinearities and/or beam-beam interaction. Analytical predictions for this interplay include the transport enhancement by resonance streaming [38]. To take a first look at such an interplay, one could measure transverse emittance growth rates due to intrabeam scattering for different values of the detuning with amplitude. Another, more exotic possibility is the suppression of intrabeam scattering by applying an rf phase modulation at three times the synchrotron frequency. Such modulation techniques have been used at synchrotron light sources to improve the Touschek beam lifetime [39]. Finally, echo signals are sensitive to diffusion or scattering processes inside the bunch [40,41]. At RHIC it may be possible to perform longitudinal as well as transverse echo experiments [5].

7 Center Frequency

An elegant technique of measuring the ring circumference, and at the same time, centering the beam orbit on average in all the sextupole magnets independently of BPM readings, is to measure the horizontal and vertical tune shifts with the rf frequency (as in chromaticity measurements) for several different sextupole excitations. Plotting the tunes versus the rf frequency, nearly straight lines are obtained (one line for each sextupole setting) which intersect at one point. The rf frequency which corresponds to the point of intersection is the center frequency, and via the beam velocity it translates into a circumference.

Such measurements were performed at DORIS and HERA by Piwinski, and at LEP by Hofmann and Schmickler [43]. An example from LEP is shown in Fig. 6.

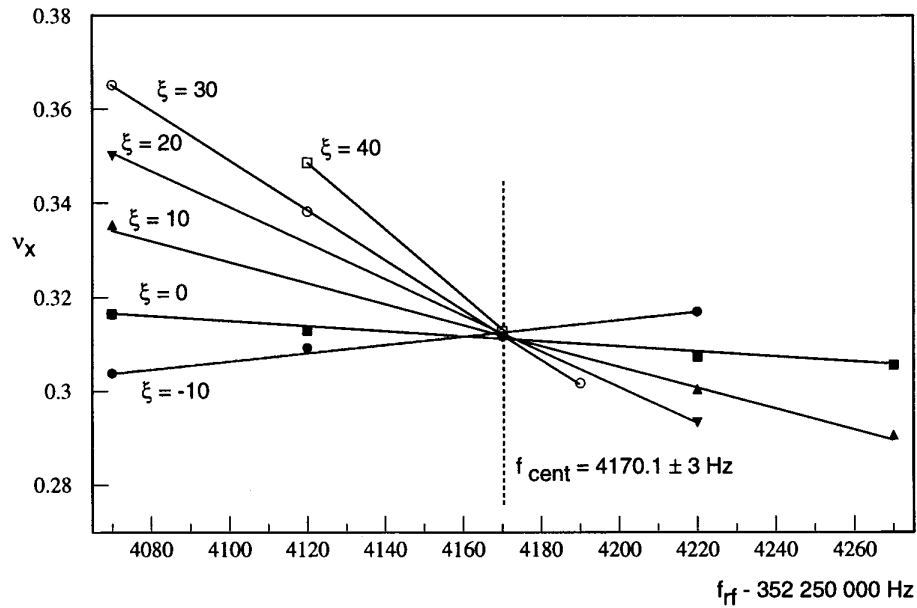


Figure 6: LEP chromaticity measurements for different sextupole excitation patterns, with net chromaticities in the range $\xi = -10$ to $+40$ [42]. The intersection of the different lines determines the central frequency, where the orbit is on average centered in the sextupoles. (Courtesy H. Burkhardt, 1998.)

Acknowledgments

We acknowledge helpful discussions with Y. Papaphilippou and J.-P. Koutchouk (on weak-strong beam-beam effects); M.P. Zorzano (on strong-strong effects); M. Furman, S. Heifets, O. Gröbner, O. Brüning, W. Stöfl, and F. Ruggiero (on the electron cloud); F. Schmidt (on the reconstruction of Hamiltonians from orbit data); A. Piwinski and H. Burkhardt (on the center frequency method). F. Zimmermann would also like to thank S. Peggs, P. Manning, M. Bai, T. Satogata, and all other members of the RHIC/AP group for making this work possible and for the hospitality experienced during his stay.

References

- [1] RHIC Design Manual, revision of April 1998.
- [2] P. Cameron et al., "The RHIC Ionization Beam Profile Monitor", IEEE PAC 1999, New York (1999).
- [3] S. Peggs and C. Tang, "Nonlinear Diagnostics Using an AC Dipole", BNL RHIC/AP/159 (1999).
- [4] M. Bai et al., "Application of the RHIC AC Dipoles and Their Expected Performance", BNL RHIC/AP/173 (1999).
- [5] O. Brüning, W. Fischer and B. Parker, "On the Possibility of Observing Transverse Echos in RHIC", BNL RHIC/AP/176 (1999).
- [6] J. Irwin, "Diffusive Losses from SSC Particle Bunches due to Long Range Beam-Beam Interactions", SSC-223 (1989).
- [7] W. Chou and D. Ritson, "Dynamic Aperture Studies During Collisions in the LHC", IEEE PAC 1997, Vancouver (1997).
- [8] Y. Papaphilippou and F. Zimmermann, "Weak-Strong Beam-Beam Simulations for the LHC", in the Proceedings of the Workshop on Beam-beam Effects in Large Hadron Colliders — LHC99, CERN-SL-99-039 (AP) (1999).
- [9] S. Peggs, "Beam-Beam Collisions and Crossing Angles in RHIC", in the Proceedings of the Workshop on Beam-beam Effects in Large Hadron Colliders — LHC99, CERN-SL-99-039 (AP) (1999).
- [10] M. Seidel, "Determination of Diffusion Rates in the Proton Beam Halo of HERA", DESY HERA 93-04 (1993).
- [11] K. Yokoya, Y. Funakoshi, E. Kikutani, H. Koiso, J. Urakawa, "Tune Shift of Coherent Beam-Beam Oscillations", KEK Preprint 92-116, and Particle Accelerators, v. 40, p. 229 (1992).
- [12] Y. Alexahin, "On the Landau Damping and Decoherence of Transverse Dipole Oscillations in Colliding Beams", CERN-SL-96-064 (AP), and Particle Accelerators v. 59, p. 43 (1998).
- [13] M.P. Zorzano, F. Zimmermann, "Coherent Beam-Beam Oscillations at the LHC", unpublished.
- [14] A. Hofmann, "Beam-Beam Modes for Two Beams with Unequal Tunes", in the Proceedings of the Workshop on Beam-beam Effects in Large Hadron Colliders — LHC99, CERN-SL-99-039 (AP) (1999).
- [15] O. Gröbner, "Beam Induced Multipacting", IEEE PAC97 Vancouver (1997).
- [16] F. Zimmermann, "A simulation study of electron-cloud instability and beam-induced multipacting in the LHC", LHC Project-Report 95, and SLAC-PUB-7425 (1997).

- [17] O. Brüning, "Numerical Simulation for the Beam Induced Electron Cloud in the LHC", EPAC98, Stockholm, LHC Project Report 190 (1998).
- [18] M. Furman, "The Electron-Cloud Effect in the Arcs of the LHC", LHC Project Report 180 (1998).
- [19] A. Drees, "Beam Induced Electron Clouds at RHIC", BNL RHIC/AP/150 (1998).
- [20] W. Fischer, "An experimental study on the long-term stability of particle motion in hadron storage rings", PhD thesis Hamburg University, DESY 95-235 (1995) and CERN SL/96-10 (AP) (1996).
- [21] O. Brüning et al., "Comparison of measured and computed dynamic aperture for the SPS and the HERA proton ring", proceedings of the LHC95 Workshop on Single Particle Effects in Large Hadron Colliders, Part. Acc. Vol. 54 pp. 223-235 and BNL RHIC/AP/84 (1996).
- [22] W. Fischer, M. Giovannozzi and F. Schmidt, "Dynamic aperture experiment at a synchrotron", Phys. Rev. E, Vol. 55, Number 3, p. 3507 (1997).
- [23] J. Jowett, "Realistic Prediction of Dynamic Aperture and Optics Performance for LEP", proceedings of the 1999 Particle Accelerator Conference, New York (1999).
- [24] J. Bengtsson, "Nonlinear Transverse Dynamics for Storage Rings with Applications to the Low-Energy Anti-Proton Ring (LEAR) at CERN", Ph.D. thesis, CERN-88-05 (1988).
- [25] J. Laskar, Physica D 67, 257 (1993); J. Laskar and D. Robin, Part. Accel. 54, p. 183 (1996).
- [26] A. Bartolini, A. Bazzani, M. Giovannozzi, W. Scandale, E. Todesco, "Tune evaluation in simulations and experiments", Part. Accel. 56, p. 167 (1996).
- [27] R. Bartolini and F. Schmidt, "SUSSIX: A computer code for frequency analysis of nonlinear betatron motion," In Lueneburg 1997, Nonlinear and stochastic beam dynamics in accelerators, pp. 390-394 (1997).
- [28] R. Bartolini and F. Schmidt, "Normal form via tracking or beam data," Part. Accel. 59, 93 (1998).
- [29] R. Bartolini, L.H. Leunissen, Y. Papaphilippou, F. Schmidt and A. Verdier, "Measurement of resonance driving terms from turn-by-turn data," CERN-SL-99-032-AP.
- [30] F. Schmidt, F. Zimmermann, H. Hayano, K. Kubo, N. Terunuma, J. Urakawa, "Analysis of Turn-by-Turn Orbit Data and Dynamic Aperture Considerations for the ATF Damping Ring", unpublished.
- [31] A. Piwinski, "Intrabeam Scattering." In Stanford 1974, Proceedings, Ninth International Conference On High Energy Accelerators, Springfield 1975, 405-409 and Hamburg Desy - INTERNAL REPORT H1-73-3 (1973).
- [32] A. Piwinski, "Intrabeam Scattering," CERN Accelerator School on Advanced Accelerator Physics, Vol. 1, p. 402 (1985).
- [33] J.D. Bjorken and S.K. Mtingwa, "Intrabeam Scattering," Part. Accel. 13, p. 115 (1983).
- [34] J. Le Duff, "Single And Multiple Touschek Effects," Presented at CERN Accelerator School, West Berlin (1987).
- [35] J. Wei, "Evolution of hadron beams under intrabeam scattering," IEEE PAC 1993, Washington, DC, p. 3651 (1993).
- [36] T.O. Raubenheimer, "The Core emittance with intrabeam scattering in e+ / e- rings," Part. Accel. 45, p. 111 (1994).

- [37] J. Tennyson, *Physica* 5D, p. 123 (1982).
- [38] A. Gerasimov, “Diffusive Transport Enhancement By Isolated Resonances And Distribution Tails Growth In Hadronic Beams,” IEEE PAC 1991, San Francisco (1991).
- [39] Yu. Senichev, N. Hertal, S. Lunt, S.P. Moeller, J.S. Nielsen. “Increasing the Life Time of SR Sources by RF Phase Modulation”, EPAC 98, Stockholm (1998).
- [40] L.K. Spentzouris and P.L. Colestock, “Coherent Nonlinear Longitudinal Phenomena in Unbunched Synchrotron Beams”, Proc. of IEEE PAC97, Vancouver, p. 16 (1997).
- [41] O. Brüning, “On the Possibility of Measuring Longitudinal Echos in the SPS”, CERN-SL-95-83 (AP) (1995).
- [42] H. Burkhardt, private communication (1998).
- [43] H. Schmickler, “Highlights from Beam Diagnostics”, EPAC96, Sitges (1996).